2022-09

Post-fire mechanical behaviour of ultra-high-performance concrete-filled steel tube (UHPCFST) stub columns under compression

Wang, T

10.1016/j.jcsr.2022.107384
Journal of Constructional Steel Research
Elsevier BV

This paper is published on:

Journal of Constructional Steel Research, *196*, 107384. doi:10.1016/j.jcsr.2022.107384

Post-fire mechanical behaviour of ultra-high-performance concrete-filled steel tube (UHPCFST) stub columns under compression

Tan Wang[a], Min Yu[a*], Xipeng Zhang[a], ShanShan Cheng[b], Sumei Liu [a]

a. School of Civil Engineering, Wuhan University, Wuhan 430072, China;
b. School of Engineering, Computing and Mathematics, University of Plymouth, PL4 8AA, UK

Abstract: Twenty-four full-scale tests were carried out in order to investigate the post-fire behaviour of UHPCFST stub columns under axial compression after being exposed to elevated temperatures. The test parameters include cross-sectional size, heating mode, steel fibre content, and coarse aggregate content. The failure modes, cross-sectional historical maximum temperatures, axial load-deformation curves, and residual compressive capacities of the specimens are analysed. The test results revealed non-uniform and nonlinear distributions of the cross-sectional historical-max temperatures. It is found that the effect of historical temperature on the residual capacity of a UHPCFST column is more obvious with the increase of the heating rate and decrease of the cross-sectional size. Inspired by the concept of average temperature method under fire, a method for calculating the post-fire residual load capacity of CFST columns was proposed based on the average historical-max temperature of the cross-section. High accuracy has been found for using the proposed calculation method, therefore the work could serve as a reference for the post-fire assessment and strengthening of UHPCFST stub columns.

Keywords: Ultra-high-performance concrete-filled steel tube; Post fire; Average temperature; Bearing capacity

Nomenclature

N_0 , $N_{T_{\max}}$	ultimate capacity of CFST column at room and after elevated temperature, respectively
$N_{s,T}$, $N_{s,T_{\max}}$	ultimate capacity of steel tube at room and after elevated temperature, respectively
$N_{c,T}$, $N_{c,T_{\max}}$	ultimate capacity of core concrete at room and after elevated temperature, respectively
A_s , A_c	area of steel and concrete, respectively
T_c , T_s	temperature of steel tube and core concrete, respectively
$\overline{T}_c$, $\overline{T}_s$	average temperature of steel tube and core concrete, respectively
$T_{c,\max}$, $T_{s,\max}$	historical maximum temperature of steel tube and core concrete, respectively
$\overline{T}_{c,\max}$, $\overline{T}_{s,\max}$	average historical maximum temperature of steel tube and core concrete, respectively
$k_{s,T}$, $k_{c,T}$	strength reduction factor of steel and concrete at elevated temperature, respectively
$\overline{k}_{c,T}$, $\overline{k}_{c,T_{\max}}$	equivalent strength reduction factor of concrete at and after elevated temperature, respectively
f_{ck} , $f_{ck,T_{\max}}$	prism compressive strength of concrete at room and after elevated temperature, respectively
f_s , $f_{s,T_{\max}}$	yield strength of steel tube at room and after elevated temperature, respectively.

1 Introduction

A building inevitably losses its original structure performance after being exposed to fire, which becomes a severe threat to the safety of human life if continuously using the damaged structure. However, demolishing buildings after fire could cause unnecessary waste of resources and environmental pollution. Therefore, evaluating the post-fire residual mechanical properties of structures is essential for sustainable development. Ultra-High performance concrete (UHPC) is usually with high strength, low porosity, and high durability [1, 2], which can effectively reduce the concrete consumption and meet the concept of 'use less and last long'. However, UHPC has low ductility [3, 4] and is likely to experience explosive spalling at elevated temperatures [5-8] , which reduces its engineering reliability. The UHPC filled steel tube (UHPCFST) is such that the UHPC is filled into the steel tube. The confinement of the steel tube prevents the core UHPC from burst and enhance the ductility of UHPC. Meanwhile, the steel tube is less likely to buckle with the support of core UHPC, which makes it easier for repairing and strengthening after elevated temperatures.

After being exposed to uniform fire, the post-fire structural performance of an UHPCFST column is related to the maximum temperature that every position of the cross-section is ever achieved during the heating and cooling phases, namely, the cross-sectional historical-max temperature field[9, 10], which is non-uniform and nonlinear within the cross-section due to the thermal inertia of concrete. Therefore, the fire-induced deterioration of concrete materials is also non-uniform and nonlinear, which brings huge challenges for predicting the post-fire structural performance of UHPCFST. Extensive studies [11-22] have been carried out on the post-fire performance of CFST structures, covering parameters such as combustion mode, fire duration, and cross-sectional size, thickness of fire protection layer, steel strength, and non-uniform fire distribution. However, the proposed empirical formula for predicting the residual load capacity of the CFST stub column was usually curve-fitted based on the tested and FEM results, which has little physical meaning, and its accuracy and scope of application are highly dependent on the quality of the regression samples. In addition, the previous studies mainly focused on the normal concrete with a strength below 80MPa. Compared to the normal strength concrete, UHPC has better thermal conductivity due to lower porosity [23, 24], thus the historical-max temperature field of the UHPCFST would be significantly different from CFST filled with normal concrete. The water in UHPC is hard to evaporate during the heating process, and the secondary pozzolanic reaction happens to the core UHPC with the unescaped water, leading to the improvement of the strength of core UHPC when the historical-max temperature is below a specific temperature (up to 600 ℃) [25-27]. Unlike UHPC, the strength of normal concrete continuously decreases with the increase of temperature. Different historical-max temperature fields and high temperature deterioration between UHPC and normal concrete will inevitably lead to the different post-fire performance. Thus, directly applying the existing research findings of normal CFST to UHPCFST would be questionable.

In order to investigate the post-fire performance of UHPCFST columns, a total of Twenty-four full-scale UHPCFST stub columns were tested under axial compression load after being exposed to elevated temperatures. The test parameters include cross-sectional size, heating mode, steel fibre content, and coarse aggregate content. The cross-sectional historical-max temperatures, axial load-deformation curves, failure modes, and residual compressive capacities of the specimens are analysed. A method for calculating residual bearing capacity of CFST columns after elevated temperatures has been proposed, where the novelty is that the residual bearing capacity is calculated based on the average historical-max temperature of the steel and concrete core cross-sections.

2 Test program

2.1 Specimen design

The research parameters include cross-sectional size, heating mode, steel fibre content, and coarse aggregate content, which affect the historical-max temperature field and post-fire behaviour of UHPCFST columns. More specifically, two

steel tube diameters (D=219mm, 377mm), two heating modes (following ISO-834 standard curve and linear heating curve), Based on our previous work on the development of UHPC containing coarse aggregate and steel fibre volume[23, 28],two levels of steel fibre content (V_{sf}=0%, 2%) and three levels of coarse aggregate content (V_{ca}=0%, 15%, 30%) were tested. As shown in Fig. 1, in T1 heating mode, the specimens were heated following the ISO-834 standard fire curve in the first 3 hours and cooled down with the rate of 4.167℃/min under ISO-834 standard heating mode, which is the recommended heating mode in codes and widely adopted by other researchers [13,31]. In addition, in T2 heating mode the specimens were heated linearly up to 1000℃ in 3 hours with the rate of 5.4℃/min and cooled down with the rate of 4.167℃/min, which is designed as a comparison to standard fire to study the post-fire behaviour of the specimen subjected to a non-standard fire. A total of Twenty-four circular UHPCFST stub columns were prepared. The specimens were labelled as S*i*CA*j*-T*k*-*m*, where S denotes the steel fibre and *i* refers to the corresponding volume fraction, CA indicates the coarse aggregate and *j* is the volume fraction, T represents the heating mode, k is the corresponding heating mode (T0 is the no heating mode, T1 refers to the ISO-834 heating mode, and T2 denotes the linear heating mode), and *m* indicates the diameter of the steel tube (219mm or 377mm). More details of the specimens can be found in Table 1.

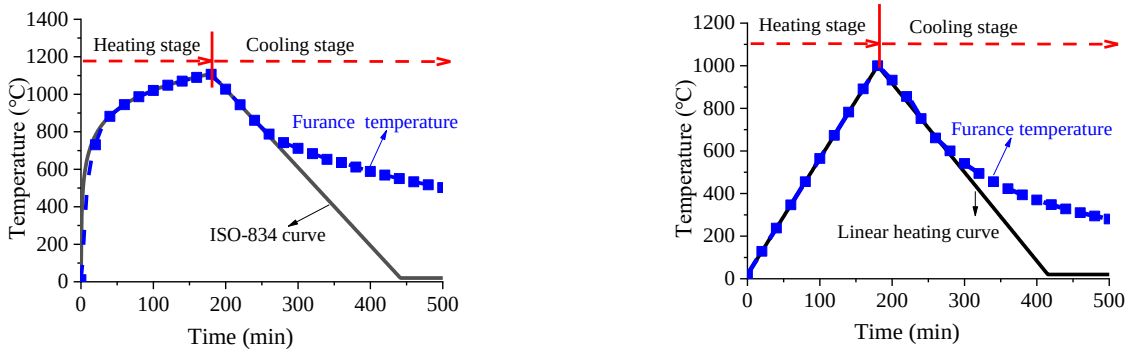

a) ISO-834 curve (T1) b) Linear heating curve(T2)

Fig. 1 Heating mode

Table 1 The details of the specimens

Specimen ID	Steel tube Dimensions			Properties	Core UHPC Volume fraction		Properties	Confinement factor ξ	Heating mode
	D(mm)	ds(mm)	H(mm)	f_s (MPa)	V_{ca}	V_{sf}	f_{cu} (MPa)		
S0CA0- T0-219	219	6	1000	440	0%	0%	85	0.50	T0
S2CA0- T0-219	219	6	1000	440	0%	2%	111	0.45	T0
S2CA15-T0-219	219	6	1000	440	15%	2%	125	0.41	T0
S2CA30-T0-219	219	6	1000	440	30%	2%	131	0.38	T0
S0CA0-T1-219	219	6	1000	440	0%	0%	85	0.50	T1
S2CA0-T1-219	219	6	1000	440	0%	2%	111	0.45	T1
S2CA15-T1-219	219	6	1000	440	15%	2%	125	0.41	T1
S2CA30-T1-219	219	6	1000	440	30%	2%	131	0.38	T1
S0CA0-T2-219	219	6	1000	440	0%	0%	85	0.50	T2
S2CA0-T2-219	219	6	1000	440	0%	2%	111	0.45	T2
S2CA15-T2-219	219	6	1000	440	15%	2%	125	0.41	T2
S2CA30-T2-219	219	6	1000	440	30%	2%	131	0.38	T2
S0CA0-T0-377	377	10	1200	354	0%	0%	85	0.56	T0
S2CA0-T0-377	377	10	1200	354	0%	2%	111	0.43	T0
S2CA15-T0-377	377	10	1200	354	15%	2%	125	0.38	T0
S2CA30-T0-377	377	10	1200	354	30%	2%	131	0.37	T0
S0CA0-T1-377	377	10	1200	354	0%	0%	85	0.56	T1
S2CA0-T1-377	377	10	1200	354	0%	2%	111	0.43	T1
S2CA15-T1-377	377	10	1200	354	15%	2%	125	0.38	T1
S2CA30-T1-377	377	10	1200	354	30%	2%	131	0.37	T1
S0CA0-T2-377	377	10	1200	354	0%	0%	85	0.56	T2
S2CA0-T2-377	377	10	1200	354	0%	0%	111	0.43	T2
S2CA15-T2-377	377	10	1200	354	0%	2%	125	0.38	T2
S2CA30-T2-377	377	10	1200	354	15%	2%	131	0.37	T2

Note: 1. H, D, and ds represent the height, diameter, and thickness of steel tube;

Note: 2. V_{ca} and V_{sf} refer to coarse aggregate and steel fibre volume fraction, respectively;

Note: 3. $\xi = (f_s \times A_s)/(f_{ck} \times A_c)$ is the confinement factor of the UHPCFST columns at room temperature, where f_s and f_{ck} are the yield strength of steel tube and the prism compressive strength of concrete, respectively; A_s and A_c are the cross-sectional area of steel and concrete, respectively.

Note: T0, T1 and T2 are no heating mode, ISO-834 heating mode, and linear heating mode, respectively.

Two types of steel tubes have been used, as shown in Fig. 2a) and dimensions presented in Table 1. 10mm thick end plates were welded at both ends of the steel tube before pouring concrete, and a hole with 100mm diameter was located in the centre of the top end plate to facilitate concrete casting. Four vent holes with the diameters of 20mm were drilled near the top and bottom of a steel tube for releasing steam pressure. Eight rib stiffeners were welded to the external wall at both ends of a column to strengthen the steel tube, thus the effect of vent holes can be eliminated. The columns were placed in an upright position and filled with concrete. An internal vibrator was used to consolidate the concrete inside the columns. The columns were left upright for 60 days before being stored horizontally at room temperature without any special curing.

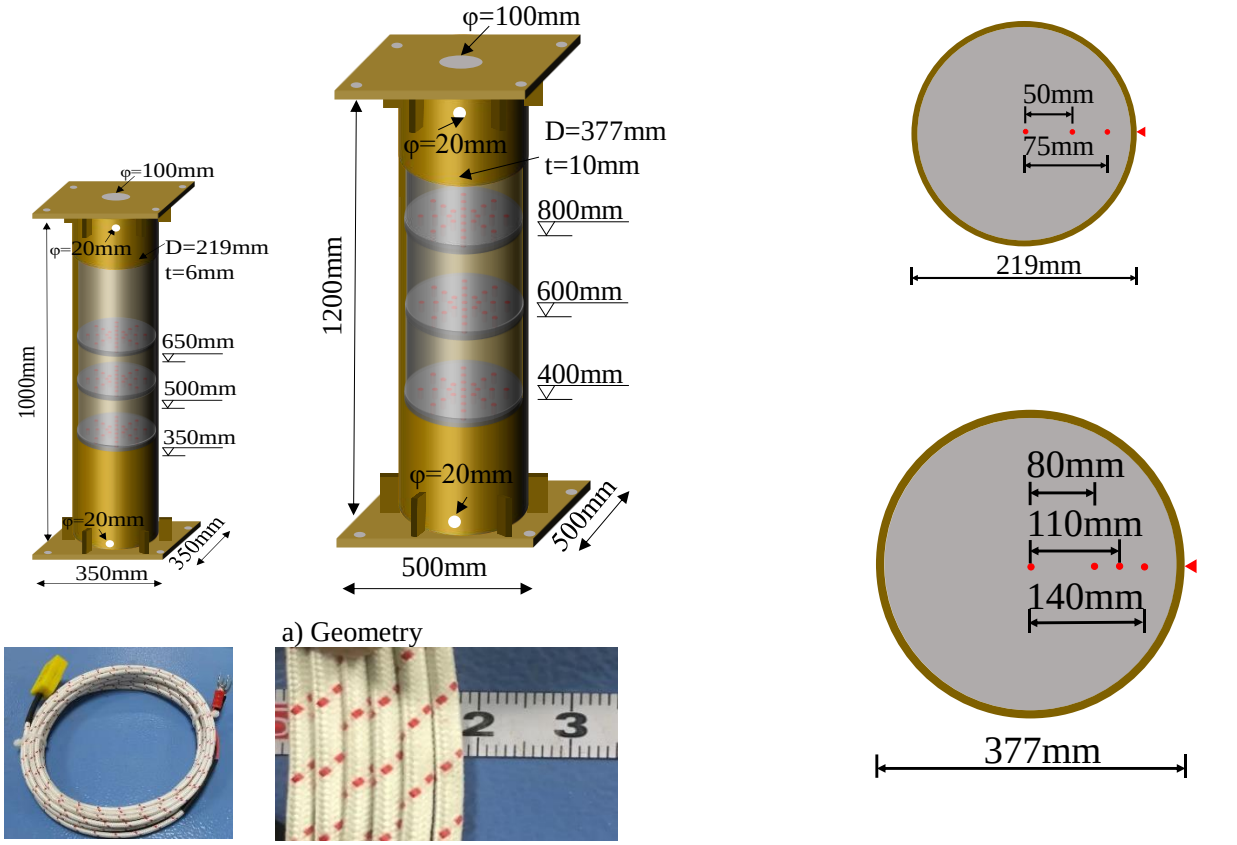

a) Geometry

c) Thermocouples

b) Temperature measurement points

Fig. 2 Specimens geometry and temperature measured points

A total of Twenty-four thermocouples have been used to measure the temperatures at different directions and heights. Locations of thermocouples within a cross-section have been demonstrated in Fig. 2 a) and b), and more details on the arrangement of the thermocouples can be found in Reference[29]. It should be noted that the diameter of thermocouples is only 3mm and the cross-sectional area of all the thermocouples account for less than 1% of the core UHPC, thus the influence of thermocouples on the mechanical behaviour of the specimens can be ignored.

2.2 Materials

The mixture proportions of UHPC adopted in this study were shown in Table 2. Among them, P.I. 52.5 Portland cement, silica fume, and fly ash were used as the binder, and the water-to-binder ratio was uniformly set as 0.17. Quartz sand with a maximum size of 0.178 mm and basalt with a diameter of 5-10 mm were used as the fine aggregate (FA) and

coarse aggregate (CA), respectively. For releasing the steam pressure, polypropylene fibres (PPF) with a volume fraction of 0.2% and a diameter of 18-48 μm was adopted, while copper coated straight steel fibres (SF) with a length of 12 mm and an aspect ratio of 45 were utilized. Finally, to improve the workability of concrete, the superplasticizer (SP) with a water reduction capability of 35% was added.

Table 2 Mixture proportions of UHPC (kg/m^3)

Mix No	Cement	Silica fume	Fly ash	water	FA	PPF	SP	SF	CA
S0CA0	875	109	109	186	1203	2	12	0	0
S2CA0	858	107	107	182	1179	2	12	157	0
S2CA15	726	91	91	154	998	2	10	157	375
S2CA30	594	74	74	126	817	2	8	157	750

Note: FA - fine aggregate, CA - coarse aggregate, SF - steel fibre, PPF - polypropylene fibre, and SP - superplasticizer.

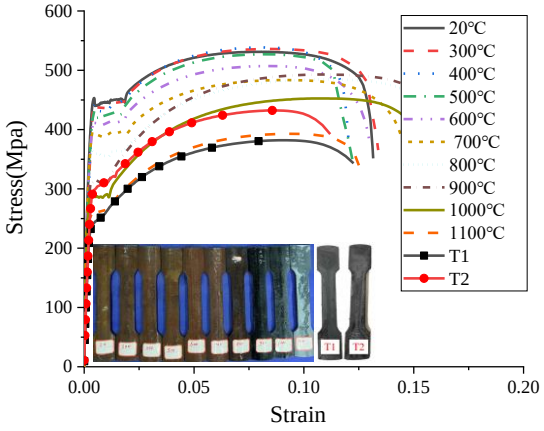

a) Stress-strain curve of steel tube(6mm)

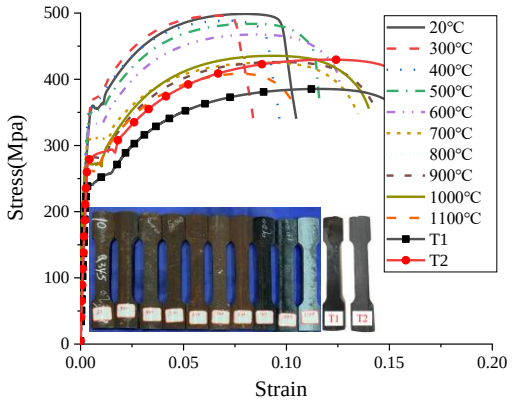

b) Stress-strain curve of steel tube(10mm)

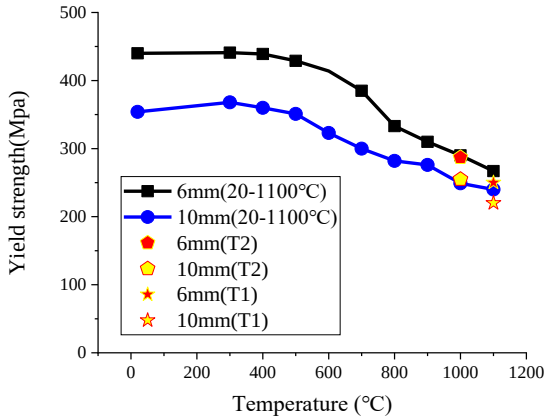

c) Tensile strength of steel

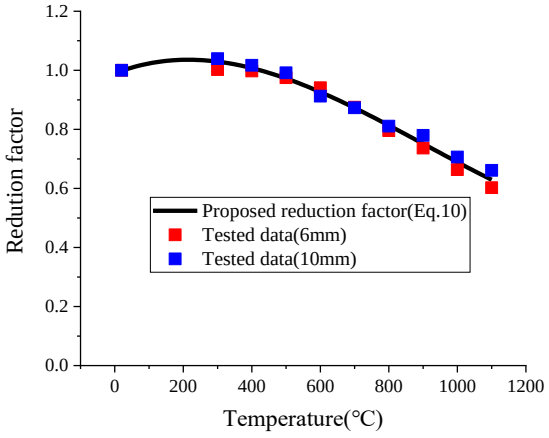

d) High temperature reduction of the steel

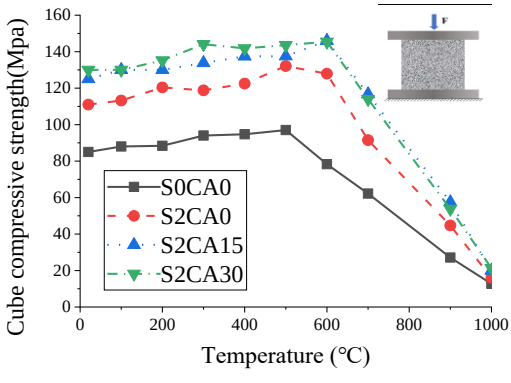

e) Cube compression of concrete

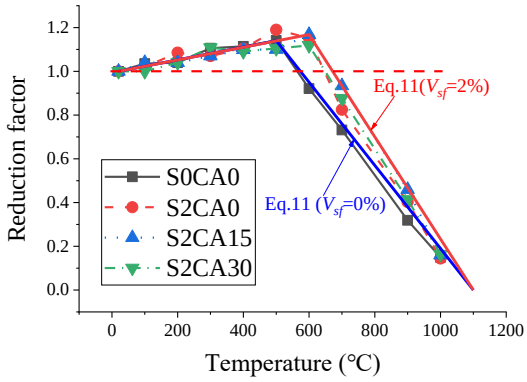

f) High temperature reduction of the concrete

Fig. 3 Material test of steel tube and concrete

According to previous research on UHPCFST at room temperature[30-33], Q345 grade steel was used for the steel tube. Steel material coupon tests were carried out at room temperature (T0), under ISO-834 heating mode (T1), linear heating mode (T2) and post fire temperatures of 300-1100℃ at 100℃ interval, where the specimens were heated up to the target temperature and held for 10 mins before cooling down. According to the requirement of standard GB/T 8162-2018[34], three repeats were adopted for each coupon test. The heated coupons were then loaded to test the residual mechanical properties of the steel after high temperature. The stress-stain curves of the steel materials are plotted in Fig. 3a) and b) and the yield strengths and the reduction factor are plotted in Fig. 3c) and d). It can be found that the post-fire residual yield strength subjected to T1 (ISO-834 heating mode) is lower than that under T2 (linearly heating mode). It is because that the austenite grain in the steel material, which reduces the residual strength of steel[35], grows more significantly under T1 mode as the period of high temperature exceeding 930 – 950 ℃ is much longer than T2.

According to the requirement of standard T/CECS 10107-2020[36], in total 120 standard concrete cubes (100mm×100mm×100mm) were tested under compression after being exposed to constant elevated temperatures up to 1000℃ for 5 hours. The cubic concrete compressive strength and their reduction factors after being exposed to different temperatures are plotted in Fig. 3c) and Fig. 3d), respectively. It can be found that The UHPC with steel fibre have higher residual strength, which contribute to that the steel fibres could improve residual mechanical properties of UHPC, and more explanation can be founded in Zheng[27].Meanwhile the standard prismatic concrete (100mm×100mm×300mm) were made to test the prismatic compressive strength of four kinds of UHPC (S0CA0, S2CA0, S2CA15 and S2CA30) at room temperature, and the corresponding strength are 72MPa, 94 MPa , 105 MPa and 111 MPa , respectively.

2.3 Test process

The whole experiments consist of the heating test and the loading test. Both the heating and loading test were conducted at the laboratory of Structural Engineering, Wuhan University. As shown in Fig. 4a), the fabricated electric furnace, capable of heating up to 1200℃ with the accuracy of ± 0.5℃ was used to heat the specimens. The heating test includes the following steps: 1) install the specimen on the support and align the axis of the specimen to the axis of the furnace; 2) cover the top and bottom end plates with refractory cotton to prevent the heat transferring from the plates, and seal the furnace; 3) heat the specimen following the designed heating modes and record the temperatures of the specimen and the furnace; 4) remove the specimen from the furnace after being cooled to room temperature. It should be noted that no external load was applied during heating as it has been found to have no significant effects on the residual strength of a structure [14]. Fig. 1 shows the comparison between the designed heating curve and the actual furnace temperature. It can be found that the furnace temperature agrees well with the designed curve at the heating stage and the early cooling stage. However, the furnace temperature drops slower than the designed curve at the later cooling stage due to the good heat-retaining properties of the furnace, which has been found to have no effect on the cross-sectional historical-max temperature.

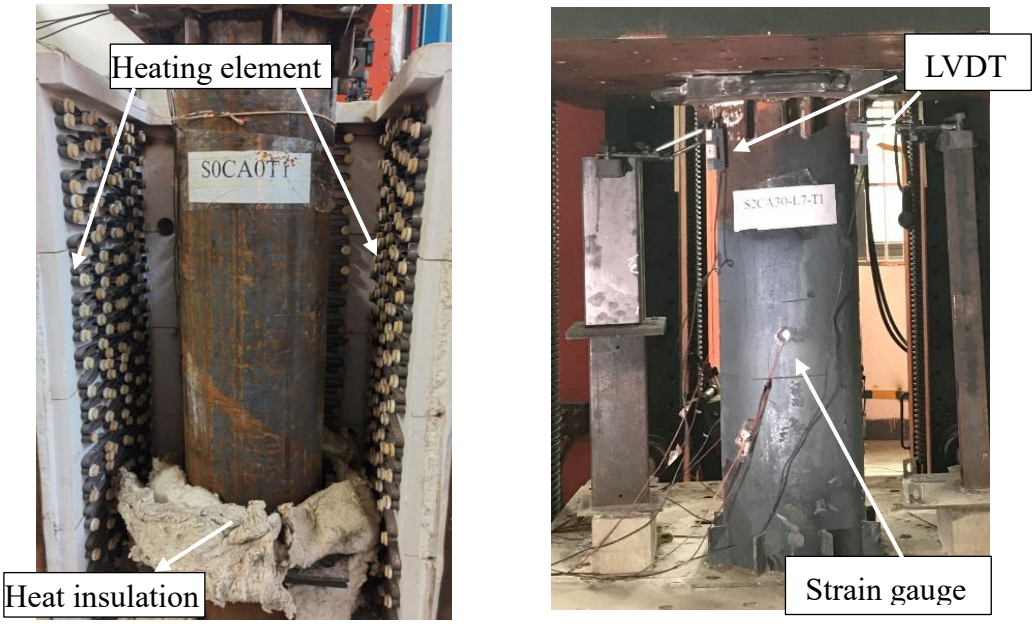

a) Heating test b) Axial compression test

Fig. 4 Test process

As shown in Fig. 4b), the electro-hydraulic servo pressure testing machine, capable of loading up to 3000kN, were used to apply an axial load to the specimens. Four linear variable differential transformers (LVDTs) were used to measure the axial deformation of the specimen. All the specimens were preloaded to check whether the load was applied centrally by comparing the measured results of the four LVDTs. The specimens were then loaded with a constant rate of 1mm/min until the compressive deformation reached up to 40000~50000με.

3 Test results and discussion

3.1 Failure modes

As shown in Fig. 5, after the heating test, the steel surface became dark and peeled due to severe oxidation and decarbonisation. Two types of failure modes were observed in the loading test: the shear failure and drum-shape upsetting failure. Under the shear failure mode, the two local bulges appear at the top and bottom of the steel tube, and a diagonal large crack can be seen after removing the steel tube. Under the upsetting failure mode, many small local bulges appear along the steel tube, and no apparent large crack can be found in the concrete.

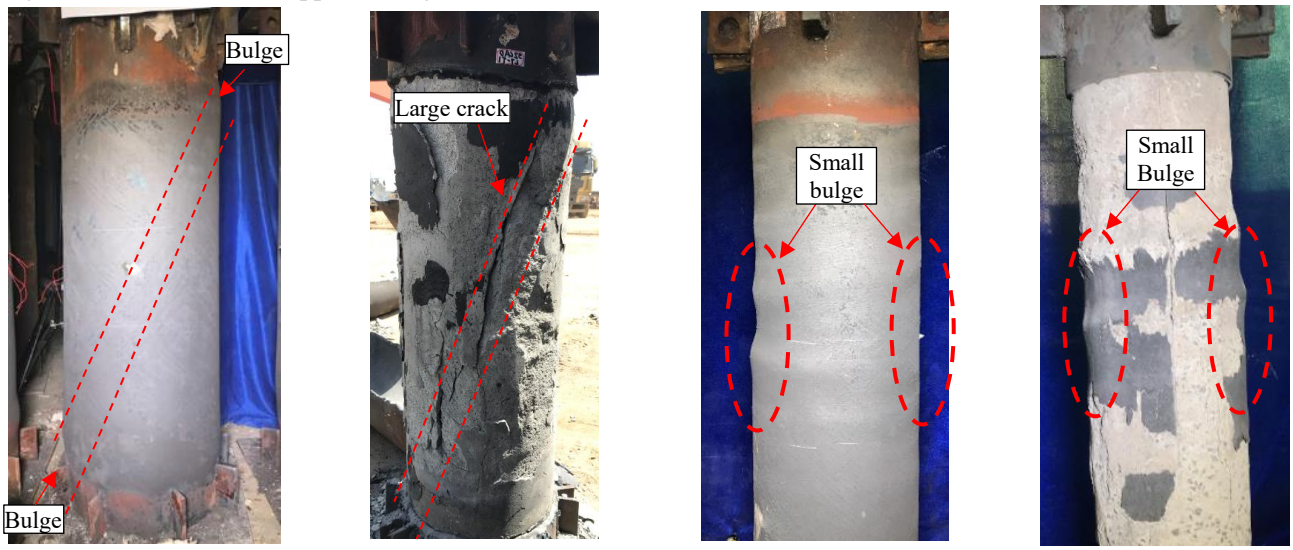

(a) Shear failure mode (b) Upsetting failure mode

Fig. 5 Failure modes of the specimens

3.2 Temperature responses

The temperatures at different depths were measured using thermocouples and averaged values are plotted in Fig. 6. It can be seen that: 1) the temperature of the steel tube generally follows the furnace temperature, although it is slightly lower than the furnace temperature at the heating stage and higher at the cooling stage; 2) the concrete core temperature continues to rise as the furnace temperature starts cooling down because of the thermal inertia of concrete; 3) the heating rate becomes small as the temperature reaches 100~150℃ due to the energy consumption of the steam evaporation, which is called the 'temperature platform', and it becomes more evident with the increase of the depth of concrete.

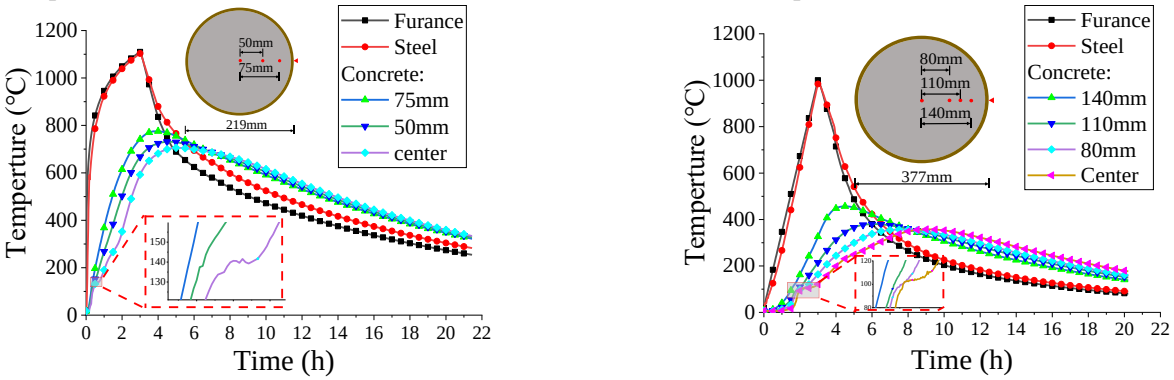

a) S0CA0T1-219 b) S0CA0T2-377

Fig. 6 Real-time temperature curves at different depths of the cross-section

The historical-max temperatures at different depths of a cross-section are presented in Fig. 7. It can be seen that the historical-max temperature distribution is non-uniform and nonlinear within the cross-section, and the nonlinearity is more obvious with the increase of cross-sectional size and decrease of heating rate. Meanwhile, the specimen with a smaller cross-section has a higher historical-max temperature for less energy consumption of core concrete. It is also found that the historical-max temperature increases with the increase of heating rate, the steel fibre content and the coarse aggregate content, due to the higher thermal driving and better thermal conductivity.

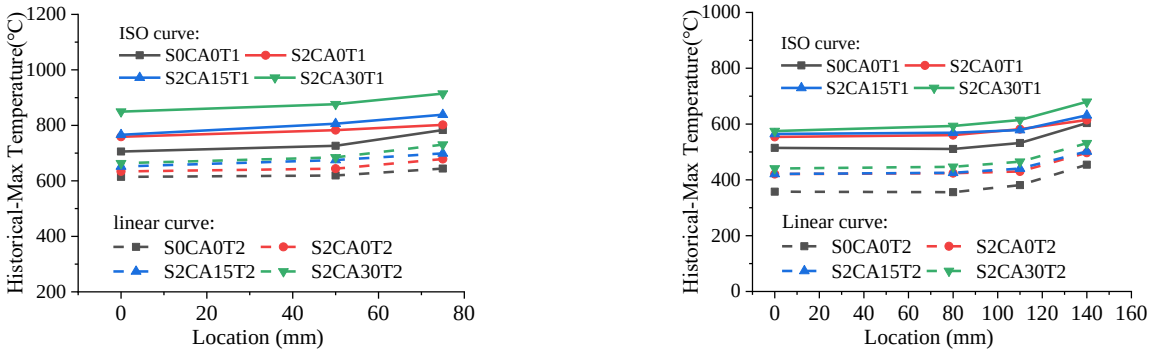

a) D=219mm b) D=377mm

Fig. 7 Historical-max temperatures at different depths of the cross-section

3.3 Load-deformation curves

Fig. 8 shows the load-deformation curves of all the tested UHPCFST columns, which are then categorised into four types as shown in Fig. 9. As for the specimens loaded at room temperature, shear failure was dominating as the confinement factor was small (ranges from 0.37 to 0.56). The load-deformation curves can be divided into four stages, 1) elastic stage (OA) where steel tube and UHPC bear loads linearly; 2) elastic-plastic stage (AB) where steel tube enters plastic stage; 3) descending stage (BC) where obvious oblique shear cracks occur to UHPC and UHPC losses its load bearing capacity gradually; 4) gentle ascending stage (CD) where core UHPC losses its load bearing capacity and the steel tube lies in the strain-hardening stage.

The cross-sectional historical-max temperature of core UHPC is usually higher than that of the normal concrete due to the higher thermal conductivity. However, the strength of UHPC increases with the increase of temperature before the critical temperature (300℃～600℃) due to secondary pozzolanic reaction, which leads to higher strength of core UHPC

compared with normal concrete. Furthermore, the historical-max temperature and strength of steel tube is nearly identical in both UHPCFST and normal CFST, which results in a lower confinement factor for UHPCFST than that of a normal CFST. As the heating mode, cross-sectional size and the strength of UHPC also have significant influence on the working mechanism of post-fire UHPCFST, the load-deformation curves of the tested columns in this paper were divided into four typical curves according to these factors. Note that this paper only focuses on stub columns, where the slenderness effect may be neglected, i.e., the slenderness ratio can be taken as zero in the equations proposed by Han and Huo[37]. Instability failure mechanism of a slender UHPCFST column is beyond the scope of this research, and further investigations would be needed.

As for specimens with large diameter (D=377mm) and lower confinement factor (ξ <0.5) under ISO-834 or linear heating mode (e.g. S2CA0T1-377, S2CA15T1-377, S2CA30T1-377, S2CA0T2-377, S2CA15T2-377, and S2CA30T2-377), the historical-max temperature was relatively low (350℃-650℃) and the strength of core UHPC after being exposed to elevated temperatures still remained relatively high, thus both the failure mode and the load-deformation curve did not differ much from those at room temperature, which is classified into Type-I.

As for specimens with large diameter (D=377mm) and relatively high confinement factor (ξ >0.5) under ISO-834 or linear heating mode (e.g. S0CA0T1-377 and S0CA0T2-377), the post-fire strength was lower than that at room temperature. The corresponding specimens showed a drum-shape failure mode (upsetting failure) and fall into Type-Ⅱ, in which the curve can be divided into three stages. Unlike Type-I, the type-II curve directly enters into gentle ascending stage (BC) after the first two stages (OA and AB) due to strong constraining effect.

As for specimens with small diameter (D=219mm), low confinement factor (ξ <0.5) under linear heating mode or the high confinement factor (ξ >0.5) under ISO-834 heating mode (e.g. S2CA0T2-219, S2CA15T2-219, S2CA30T2-219, and S2CA30T1-219), the historical-max temperature of core UHPC was relatively high (600-700℃ for linear heating mode; 700-900℃ for ISO-834 heating mode). The residual strength of core UHPC was relatively high and the specimens showed shear failure. However, the residual stiffness of the core UHPC was very low, thus the steel tube shared more compression load and yielded early. Similar to Type-I, the corresponding curve can be divided into four stages and classified into Type-III. The difference is that the elastic stage is shorter and the elastic-plastic stage is longer.

As for specimens with small diameter (D=219mm), high confinement factor (ξ >0.5) under linear heating mode or the low confinement factor (ξ <0.5) under ISO-834 heating mode (e.g. S0CA0T1-219; S2CA0T1-219; S2CA15T1-219; S0CA0T2-219), both the residual stiffness and strength of the core UHPC were every small. The steel yielded early and the specimen showed the drum-shape upsetting failure mode. The corresponding curve can be classified into Type-Ⅳ where the curve is divided into three stages like Type-Ⅱ, and the difference also lies in the longer elastic-plastic stage of Type-Ⅳ.

From analysis above, it can be found that as the temperature of core UHPC is relatively low (e.g. average temperature is below 600℃), the confinement factor of a post-fire UHPCFST column is smaller in comparison with that at room temperature, and the load bearing capacity of the column will decrease after the stress of core UHPC reaches the peak value, due to limited confinement effect provided by the outter steel tube, leading to shear failure mode in the post-fire UHPCFST columns. However, as for normal CFST columns, the confinement factor increases due to continuous decrease of the strength of core concrete, thus the load capacity of the column still increases after the stress of core concrete reaches the peak value, which eventually leads to drum-shape upsetting failure mode. When the temperature of core concrete is higher than 600℃, the reduction of residual post-strength of both UHPC and normal concrete is relatively small, so the confinement effect is very strong. Both UHPCFST and normal CFST show similar behaviour.

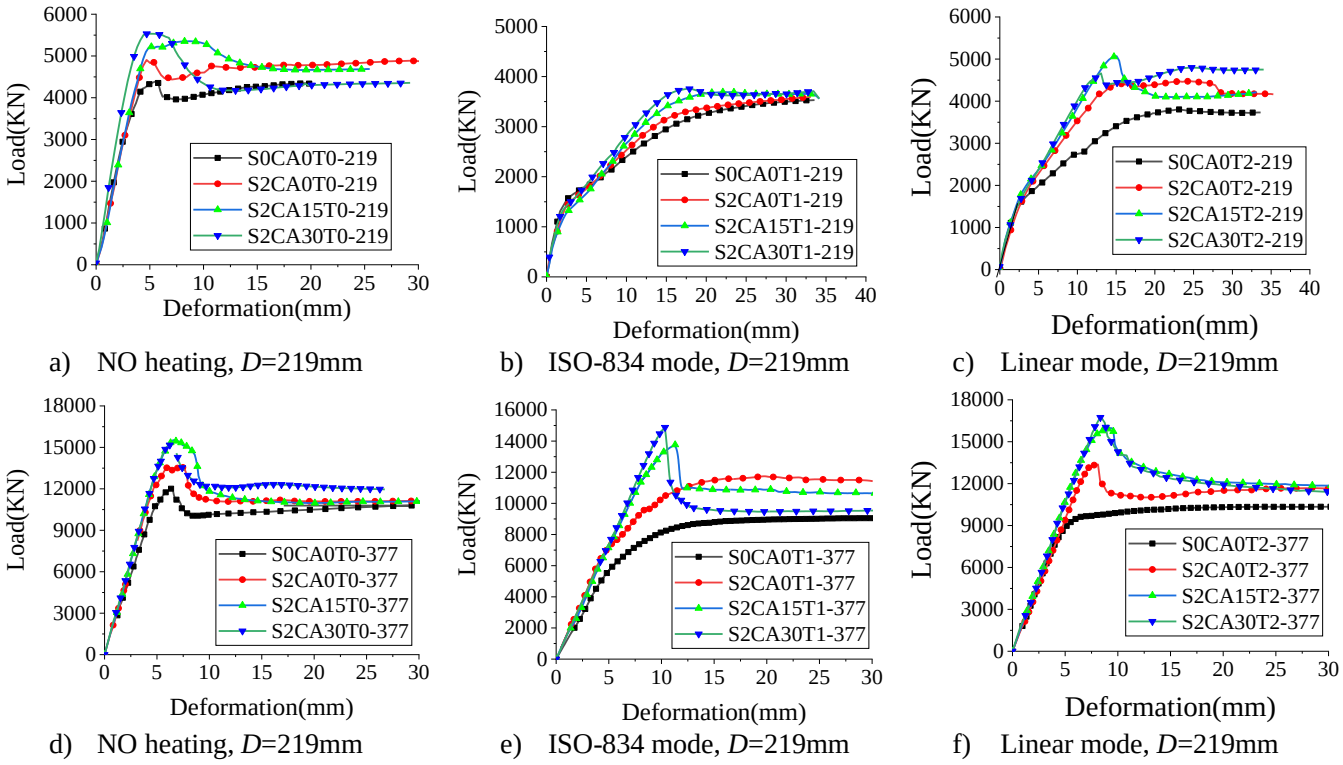

a) NO heating, *D*=219mm b) ISO-834 mode, *D*=219mm c) Linear mode, *D*=219mm

d) NO heating, *D*=219mm e) ISO-834 mode, *D*=219mm f) Linear mode, *D*=219mm

Fig. 8 Load-deformation curve of UHPCFST columns

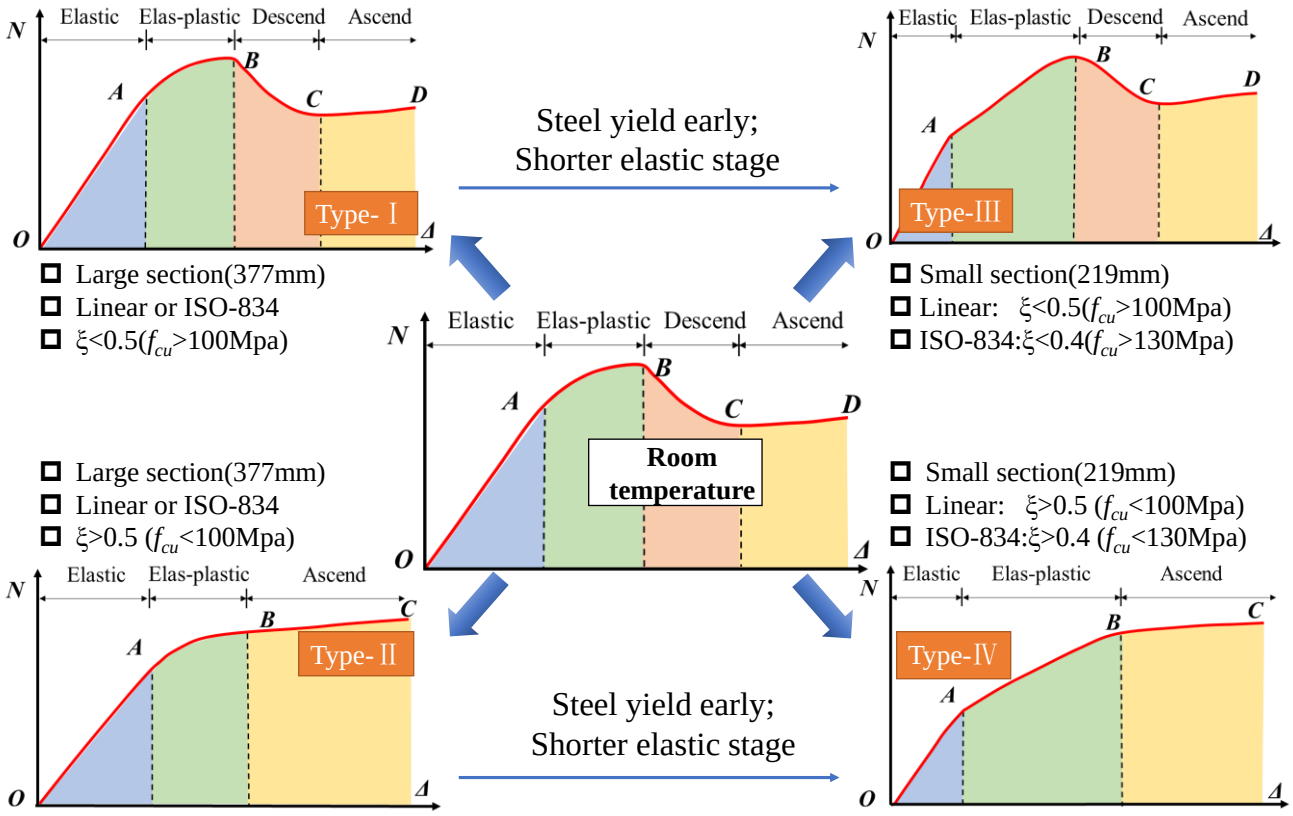

Fig. 9 Typical load-deformation curves of UHPCFST columns

3.4 Residual bearing capacity

The post-fire residual bearing capacity of the UHPCFST column ($N_{T_{max}}$) is one of the most important index for evaluating the post-fire performance of an UHPCFST column. As for the specimens with obvious descending stage, the $N_{T_{max}}$ is defined as maximum ultimate load and the $N_{T_{max}}$ is determined by furthest point method [38] for the specimens

without obvious turning. To facilitate the assessment of residual bearing capacity, residual strength index (k_{rei}) is defined as Eq.(1) [37]:

$$k_{rei}=\frac{N_{T_{max}}}{N_0} \tag{1}$$

where N_0 is the bearing capacity of the UHPCFST column at room temperature.

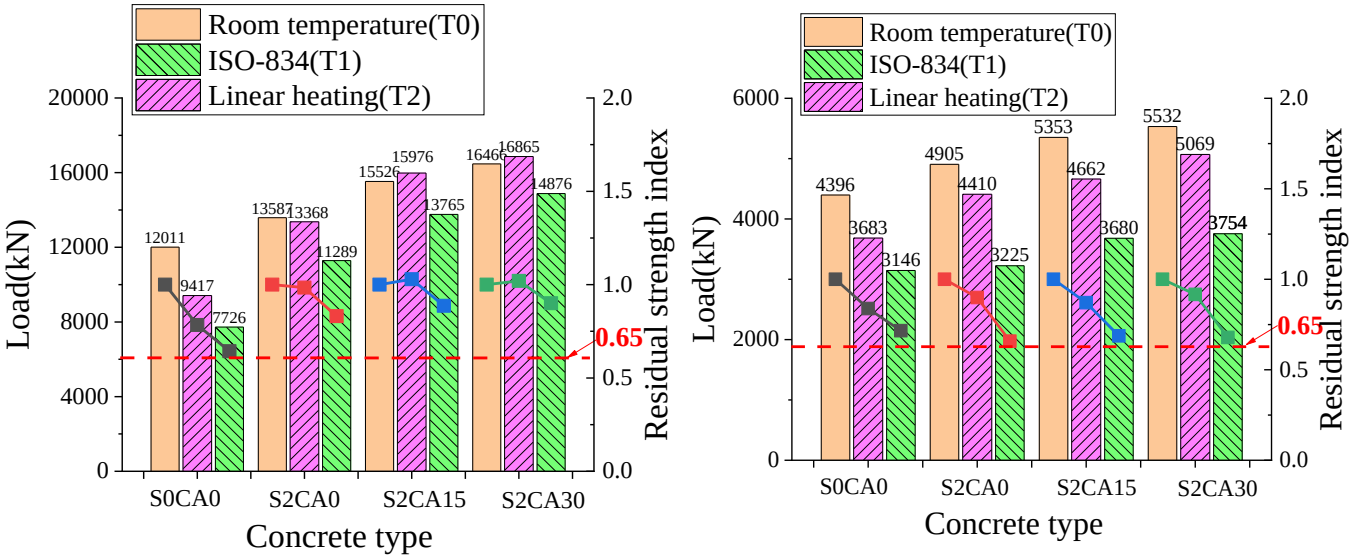

a) D=377mm b) D=219mm

Fig. 10 Residual bearing capacity and residual strength index of UHPCFST

The residual bearing capacity and residual strength index of UHPCFST columns are shown in Fig. 10. It can be found that the residual strength index of specimens under T2 (linear heating mode) is higher than that under T1 (ISO-834 heating mode) due to its lower historical temperature. The residual strength index of some specimens under T2 is around 1, indicating that the UHPCFST column did not lose its compressive bearing capacity although the environment temperature has reached 1000℃. It can be mainly attributed to that the historical-max temperature of most zones in concrete did not exceed 500℃ (as shown in Fig. 7b) due to thermal inertia[23]. The strength of UHPC increased with the increase of temperature before the critical temperature (300℃～600℃) due to secondary pozzolanic reaction, as Peng[39] recently found that a high temperature steam environment established in the inner part of a UHPC specimen results in the transformation of C-S-H gels to crystals, leading to the improvement of concrete compressive strength. It is also found that the specimens with smaller cross-sectional size have the lower residual bearing capacities, which is because that the historical-max temperature of the smaller cross-section is higher (most zones in concrete core lie in 600℃~900℃) due to less energy consumption of core concrete. In addition, the specimens with steel fibre had higher residual strength than those without steel fibre, due to the higher critical temperature for the UHPC with steel fibre (as shown in Fig. 3d). The residual strength index of all the specimens exceeded 0.65 after being exposed to elevated temperatures up to 1000℃ for at least 3 hours, indicating that the UHPCFST columns have adequately high residual bearing capacity. As the residual strength index of a normal CFST could drop to 0.6 after being exposed to ISO-843 standard fire for a shorter period (1.5 hours)[16], adopting the same design method of a normal CFST to a UHPCFST would be over conservative, thus the post-fire design method of UHPCFST columns should be improved.

4 Calculation method of residual capacity of UHPCFST stub columns

4.1 Calculation method based on average historical-max temperature

A): Historical-max temperature field

In this research, the post-fire residual strengths of steel tube and core concrete are defined using their cross-sectional historical-max temperature field. As shown in Eq.(2) and Fig. 11, the historical-max temperature is taken as the maximum temperature of all the positions (*x, y*) during the whole heating and cooling period. It can be found that the historical-max temperature within the steel tube is relatively uniform due to its good thermal conductivity and thin wall thickness. However, the temperature field within the core concrete is highly non-uniform and nonlinear due to its low thermal conductivity and large diameter.

$$T_{\max} = \max\left\{T(x,y,t),t\right\} \tag{2}$$

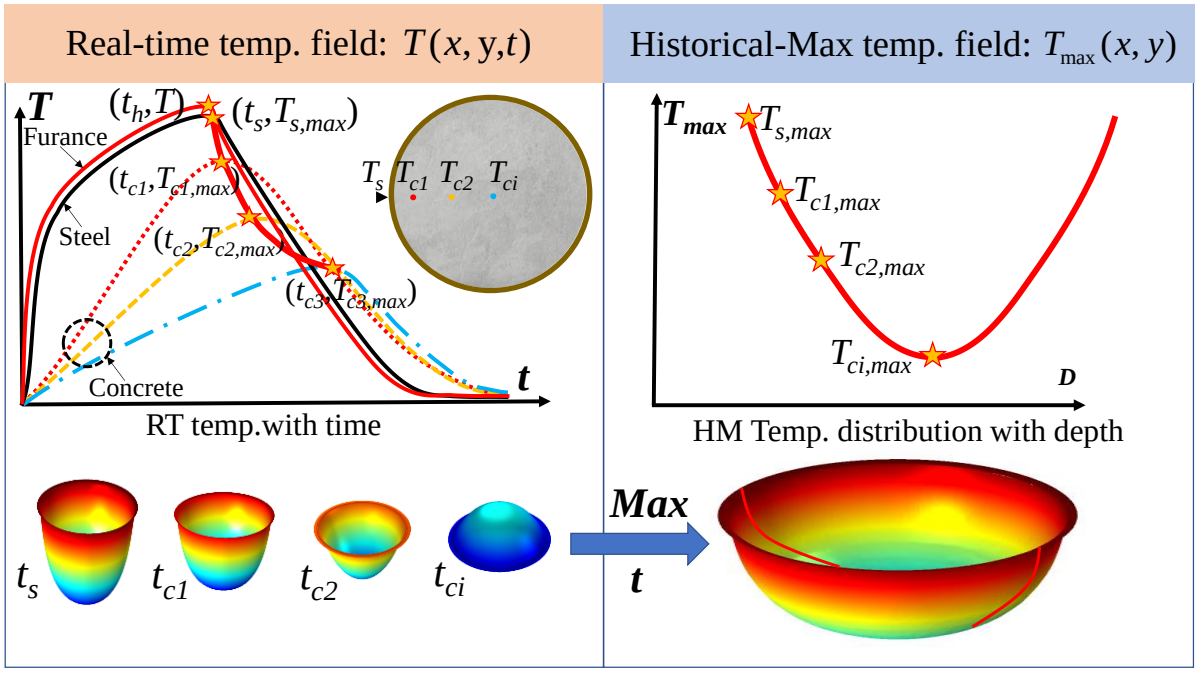

Fig. 11 The method for obtaining the historical-max temperature field of CFST

B): The calculation of equivalent strength based on average historical-max temperature

The non-uniform and nonlinear historical-max temperature inevitably causes nonlinear reduction on the residual strength of UHPC, which brings huge challenges when predicting the residual strength of the CFST structure after fire. Taking advantage of an equivalent uniform reduction is a sensible simplified method. In the author's previous work[40], the strength of steel tube and core concrete under fire were calculated on the basis of the average real-time temperature of the cross-section. The schematic diagram of temperature equivalent process is presented in Fig. 12. It can be seen that the non-uniform temperature field within the steel tube or core concrete under elevated temperature $T_\alpha(\mathrm{x},\mathrm{y})$ are equivalent to the cross-sections with uniform temperature field $\bar{T}_\alpha$ by taking the average value of the non-uniform temperature within the section, where the subscript α takes *s* for steel tube and *c* for concrete core. The ultimate capacity $\bar{N}_{\alpha,T}$ and the equivalent strength $\bar{f}_{\alpha,T}$ of steel tube or core concrete at elevated temperatures can be obtained as below:

$$\overline{N}_{\alpha,T} = \overline{f}_{\alpha,T} A_\alpha,\ \overline{f}_{\alpha,T} = \overline{k}_{\alpha,T}\left(\overline{T}_\alpha\right) f_\alpha \tag{3}$$

where A_α is the cross-sectional area, f_α is the material strength (yield strength for steel and prismatic compressive strength for concrete) at room temperature, and $\bar{k}_{\alpha,T}$ is the equivalent reduction factor of material strength at high temperature. More details can be found in Ref [40-43].

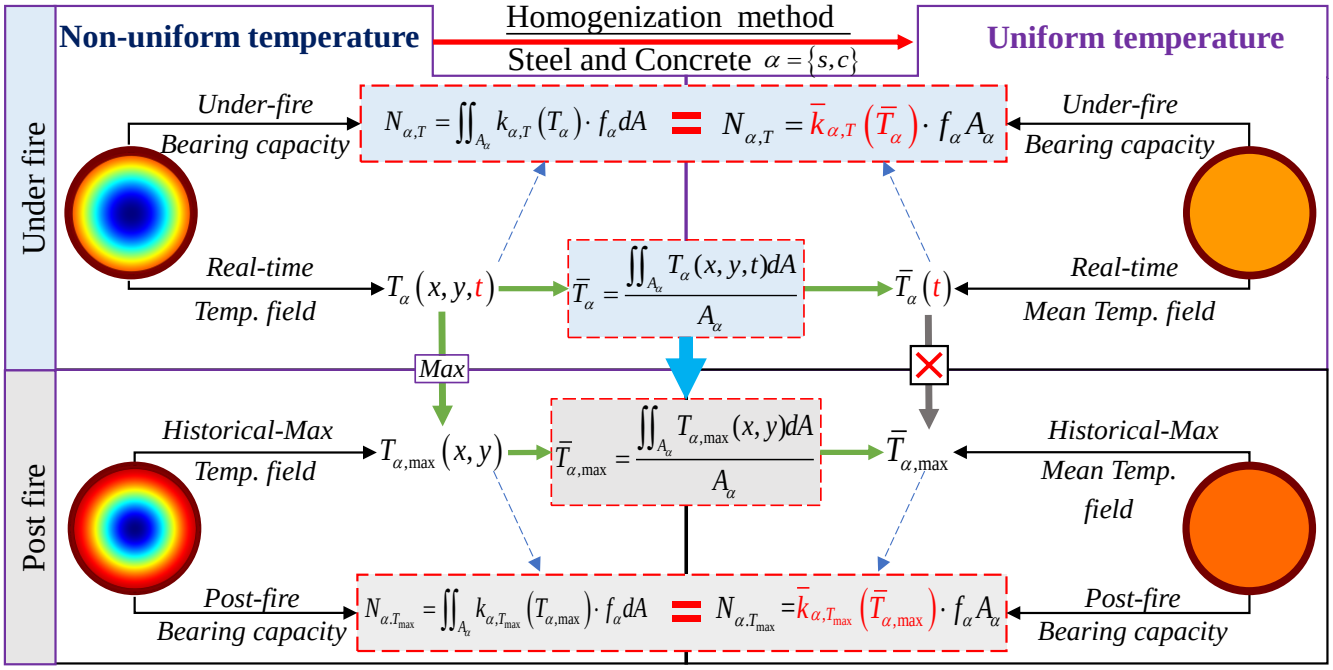

Fig. 12 Schematic diagram of temperature equivalent process

The average historical-max temperature $\bar{T}_{\alpha,max}$ can be expressed as Eq.(4).

$$\bar{T}_{\alpha,\max}(t)=\frac{\iint_{A_\alpha}T_{\alpha,\max}(x,y,t)dA}{A_\alpha} \tag{4}$$

In analogy with the method for calculating the equivalent strength of steel tube and concrete at elevated temperatures, the equivalent post-fire strength of steel tube and core concrete after being exposed to elevated temperature can be expressed as Eq.(5).

$$\bar{f}_{\alpha,T_{\max}}=\bar{k}_{\alpha,T_{\max}}\left(\bar{T}_{\alpha,\max}\right)f_\alpha \tag{5}$$

where $\bar{k}_{\alpha,T_{max}}$ is the post-fire equivalent material reduction factor and can be expressed as Eq.(6).

$$\bar{k}_{\alpha,T_{\max}}\left(\bar{T}_{\alpha,\max}\right)=\frac{\iint_{A_\alpha}k_{\alpha,T_{\max}}\left(T_{\alpha,\max}(x,y)\right)dA}{A_\alpha} \tag{6}$$

C): Calculation process of the residual capacity

It is assumed that a formula for calculating the post-fire residual capacity of a CFST column takes the same structure as that at room temperature. Based on the assumptions as presented in Fig. 13, the formula of load bearing capacity of CFST at room temperature ($N_{u,0}$) can be extended to calculate the post-fire load bearing capacity ($N_{u,T_{max}}$) by replacing material strength at room temperature with the equivalent material strength after elevated temperatures. Eventually, the formulae of the bearing capacity of a CFST at room temperature and after elevated temperatures were unified.

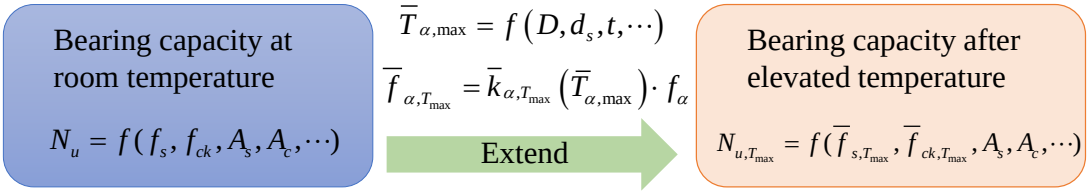

Fig. 13 The process of calculating the bearing capacity of CFST columns after elevated temperature

4.2 The calculation of the average historical-max temperature and equivalent strength

4.2.1 Average historical-max temperature of steel tube and core UHPC

The heat transfer module embedded in COMSOL Multiphysics were used to simulate the real-time temperature field. "Domain ODEs and DAEs" module in COMSOL Multiphysics were adopted to calculate the maximum historical temperature field, where a variable $T_{temp}(x,y,t)$ was set to save the maximum temperature of the position (x, y). If $T(x,y,t) > T_{temp}(x,y,t)$, $T_{temp}(x,y,t) = T(x,y,t)$. Eventually the maximum historical temperature is saved to $T_{temp}(x,y,t)$, namely, $T_{max}(x,y) = T_{temp}(x,y,t_{final})$,in which t_{final} refers to the moment when the temperature cools down to the room temperature. The thermal parameters of four kinds of UHPC tested by our research group [23] and steel proposed by TTL [44] was adopted, respectively. The heating curve follows the actual tested temperature, and more details of the heat transfer model for CFST columns in fire are presented in Yu et al. [45]. The time-dependent temperature curves and the historical-max temperatures of numerical and experimental specimens are compared in Fig. 14. It can be found that both simulated real-time temperature and historical-max temperature agree well with the tested results, indicating that the FEM model is adequate to simulate the cross-sectional historical-max temperature field. Eventually, the average historical-max temperatures of steel tube and core concrete can be calculated using Eq.(6), based on the simulated historical-max temperature field.

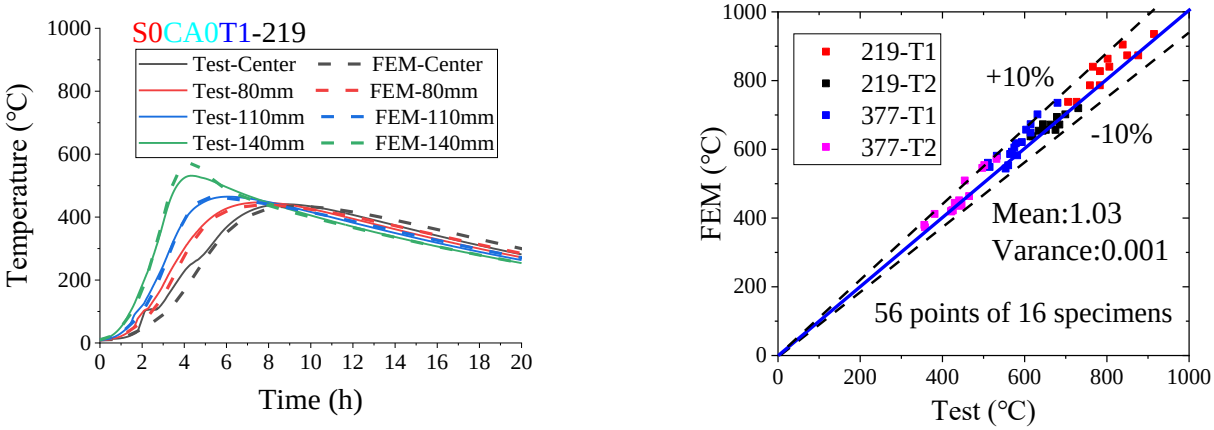

a) Real-time temperature b) Historical-max temperature

Fig. 14 The comparison of the temperature between test and simulation

In the parametric studies on average historical-max temperature of CFST columns, a series of cross-sectional size, the mixture of the UHPC, heating mode and heating-up time were considered. The geometric parameters include six steel tube thicknesses (3, 9, 15, 21, 27, 33mm), and six steel tube diameters (100, 200, 300 400, 500, 600mm), respectively. The mixture of the UHPC consists of S0CA0, S2CA0, S2CA15 and S2CA30 as described in Section 2.2. The ISO-834 and linear heating mode are considered, and the temperatures were recorded every five minutes ranging from 0 to 180min. In total there are 10368(6×6×4×2×2×36) numerical cases were designed.

A): Steel tube

As shown in Fig. 15, steel tube had little difference between the average real-time temperature and the historical-max temperature, especially for the specimens with small thickness of steel tube. It is because that the temperature of the steel tube immediately dropped as the furnace temperature started cooling down due to its good thermal conductivity and relatively thin thickness. In authors' previous work[41], the formula of the $\bar{T}_s$ was given as expressed in Eq.(8) under ISO-834 heating mode. Meanwhile, the incremental method for calculating the average temperature of steel tube for any heating mode (e.g. linear heating mode) also can be found in authors' previous work [46].

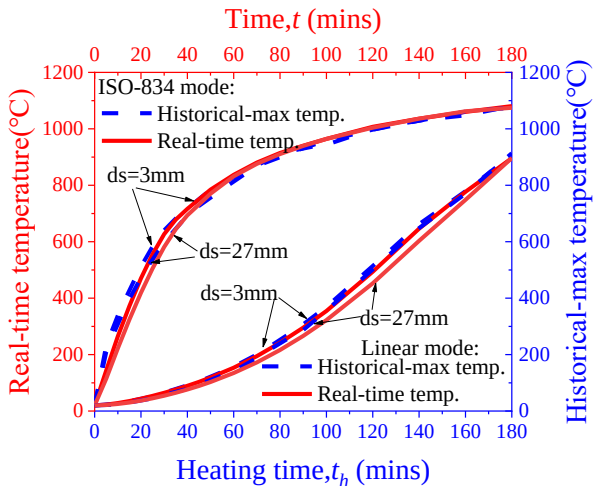

a) D=300, ds=6mm, SCA30

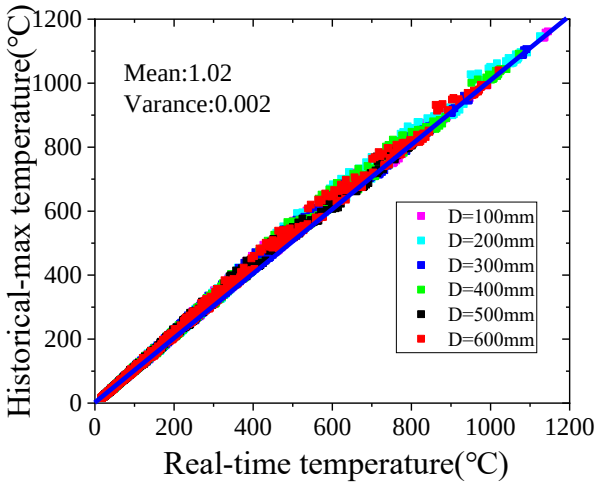

b) All cases

Fig. 15 Comparison between historical-max temperature and real-time temperature of steel tube

$$\overline{T}_{s,\max}(t_h) \cong \overline{T}_s(t) \tag{7}$$

$$\overline{\theta}_{s.\max}(t_h) = \overline{T}_{s,\max} - T_0 = \overline{T}_s - T_0 = \eta_s \theta_f = \frac{(mt_h)^{A_s}}{(mt_h)^{A_s} + B_s}\theta_f \tag{8}$$

where θ_f represents the elevated temperature of fire, which is defined as $\theta_f = 345\log 10(8t_h + 1)$ under ISO-834 fire; $A_s = 1.15 + 0.0043d_s$ and $B_s = 0.5(d_s + 20)$, where d_s is the thickness of steel tube in millimetre; m is taken as 1, 1.15, 1.2, and 1.3 for S0CA0, S2CA0, S2CA15 and S2CA30, respectively.

B): Concrete

Inspired by Wickström[47] and Yu[41], the ratio of the zero-centred average historical-max temperature of concrete and that of steel tube $\eta_c = \bar{\theta}_{c,max}/\bar{\theta}_{s,max}$ between ISO-834 heating mode and linear heating mode are compared in Fig. 16 a). It can be found that the temperature ratio (η_c) under the two-heating mode is very close to each other regardless of the cross-sectional size. Fig. 16 b) plots the simulated η_c against the unified hating-up time $t_{h,w} = t_h/(d_c)^5$ (where d_c is the concrete core diameter in millimetre). The η_c of the different cases show same trend, therefore the average historical-max temperature of core UHPC was proposed as Eq.(9), using the simulated results.

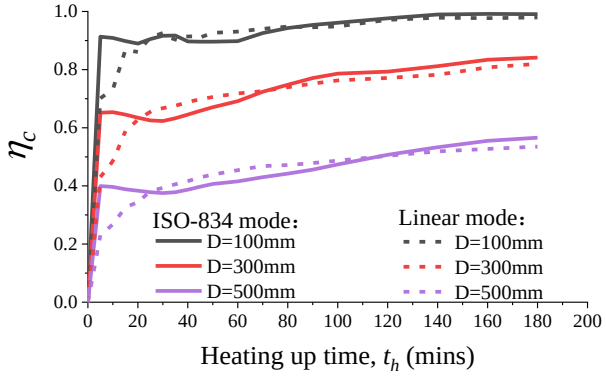

a) η_c vs time

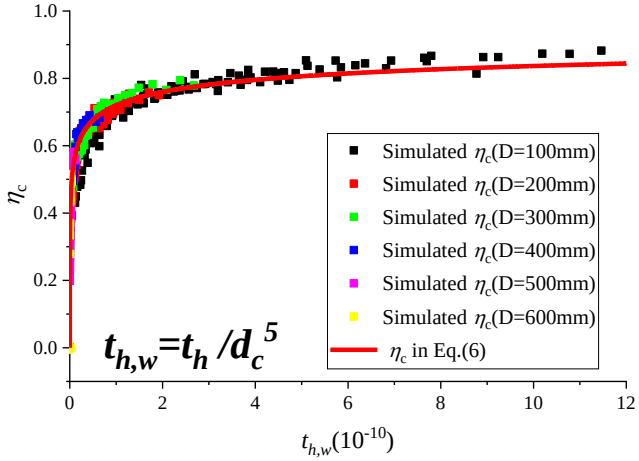

b) η_c vs $t_{h,w}$

Fig. 16 Temperature ratio η_c for different cases

$$\bar{\theta}_{c.\max} = \bar{T}_{c,\max} - T_0 = \eta_c(t_h)\bar{\theta}_{s,\max}$$

$$\eta_c(t_h) = \frac{\bar{\theta}_{c,\max}}{\bar{\theta}_{s,\max}} = \frac{\left(nt_{h,w}\right)^{A_c}}{\left(nt_{h,w}\right)^{A_c} + B_c} \tag{9}$$

where $A_c = 0.3; B_c = 0.00035$; n is related to the thermal conductivity of the core concrete, which is taken as 1, 1.5, 2.8, and 3 for S0CA0, S2CA0, S2CA15 and S2CA30, respectively. The average historical-max temperature of steel tube and core UHPC are compared in Fig. 17. It can be found that the results for both steel and concrete agree with each other very well.

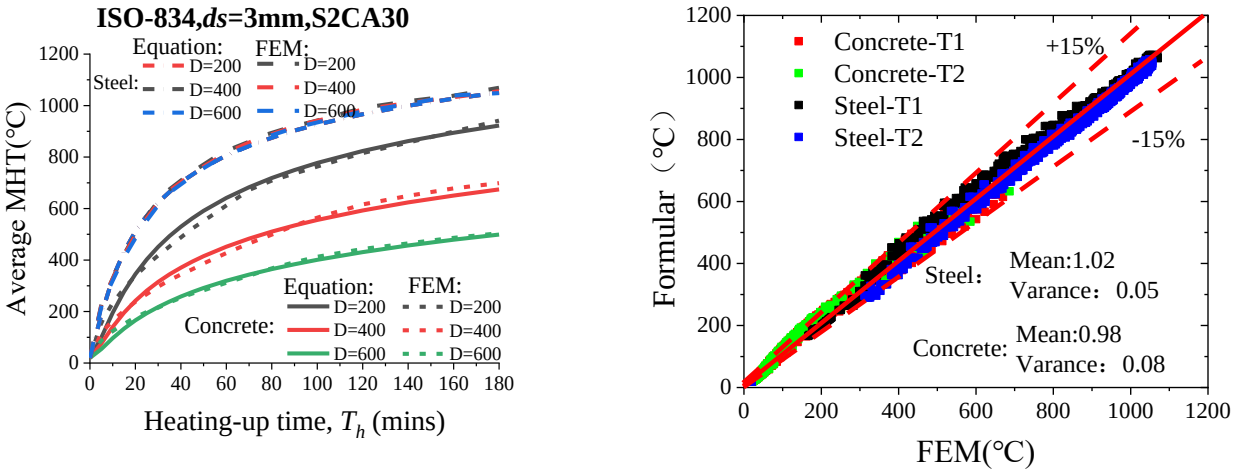

a) Reprehensive cases b) All cases

Fig. 17 Average historical-max temperature between formula and FEA

4.2.2 Equivalent strength of steel tube and core UHPC after elevated temperatures

A): Steel tube

As for steel tube, the temperature field is relatively uniform, namely, $\bar{T}_{s,max} = T_{s,max}(x,y)$, so is the material reduction factor. Based on the tested data (shown in Fig.3c), the post-fire reduction factor of the residual strength of steel is proposed, as expressed in Eq.10. It should be noted that, although the period of the high temperature exceeding 930–950℃ influences the residual mechanical properties of steel, the effect is rather limited. For simplicity, it is assumed that the residual mechanical properties of steel tube only depend on the peak temperature of the heating curve.

$$k_{s,T_{\max}} = 0.43\times\left(\frac{T_{\max}}{1000}\right)^3 - 1.18\times\left(\frac{T_{\max}}{1000}\right)^2 + 0.44\times\left(\frac{T_{\max}}{1000}\right) + 0.99,\ \ 20℃ < T_{\max} < 1100℃ \tag{10}$$

As expressed in Eq.(5), the equivalent yield strength of steel tube after elevated temperature ($\bar{f}_{s,T_{max}}$) can be obtained by multiplying yield strength at room temperature (f_s) by the high temperature equivalent reduction factor.

B): Concrete

Based on the cube compression test results of the UHPC after elevated temperatures (described in section 2.2), the high temperature reduction factor as expressed in Eq.(11) was proposed:

$$k_{c,T_{\max}} = \begin{cases} 0.29\dfrac{T_{\max}-20}{1000} + 1 & (T_{\max} \le T_{cr}) \\ k_{c,T_{cr}}\left(\dfrac{1100-T_{\max}}{1100-T_{cr}}\right) & (T_{\max} > T_{cr}) \end{cases} \tag{11}$$

where T_{cr} is the critical temperature that the UHPC strength starts dropping, which is taken as 500℃ and 600℃ for the UHPC with steel fibre content of 0% and 2%, respectively.

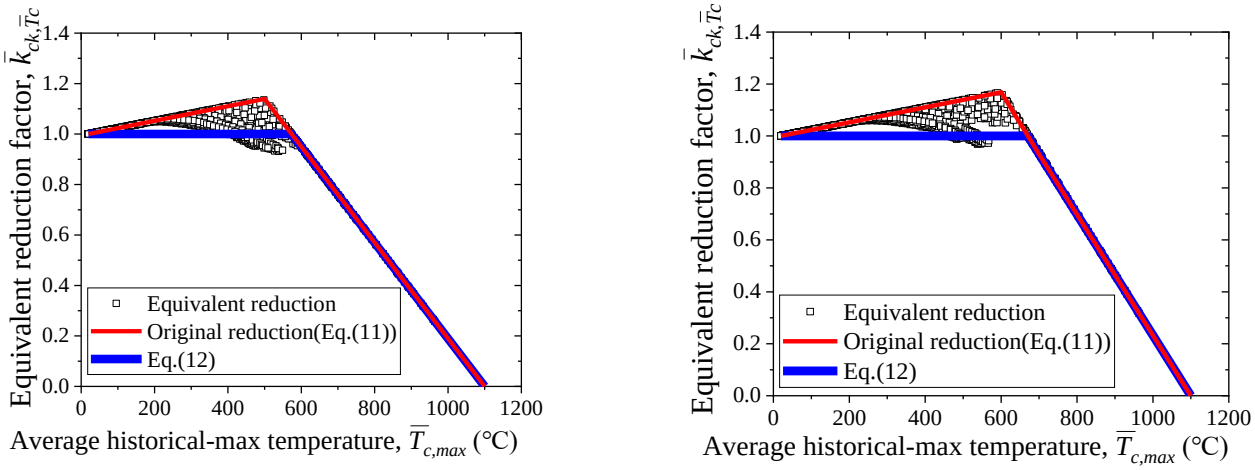

Fig. 18 Equivalent reduction factors of UHPC strength under high temperatures

Fig. 18 compares the equivalent high temperature reduction factor with its corresponding original reduction factor. It should be noted that the square nodes in Fig 18 were obtained by calculating the average historical-max temperature $\bar{T}_{c,max}$ and the post-fire equivalent material reduction factor $\bar{k}_{\alpha,T_{max}}$ of designed simulation cases (10368 cases) as presented in section 4.2.1. For each case, the specific steps are as follows:1) The historical-max temperature field $T_{c,max}(x,y)$ was obtained by COMSOL; 2) The value of the average historical-max temperature $\bar{T}_{c,max}$ of core UHPC was obtained by integral operation in post-process of COMSOL according to Eq.4;3) The value of the equivalent material reduction factor $\bar{k}_{\alpha,T_{max}}$ of core UHPC were obtained by integral operation in post-process of COMSOL according to Eq.6; Point（$\bar{T}_{c,max}$，$\bar{k}_{\alpha,T_{max}}$） is the one of the square nodes in Fig.18. It can be found that the equivalent high temperature reduction factor is smaller than its corresponding original reduction factor when the historical-max temperature is lower. To achieve a safer design, a new two-piecewise linear function is introduced to calculate the equivalent reduction factor of concrete strength, as expressed by Eq.(12):

$$\bar{k}_{c,T_{\max}}=\begin{cases}1 & (\bar{T}_{\max}\le 1100-\dfrac{1100-T_{cr}}{k_{c,T_{cr}}})\\ k_{c,T_{cr}}\left(\dfrac{1100-\bar{T}_{\max}}{1100-T_{cr}}\right) & (\bar{T}_{\max}>1100-\dfrac{1100-T_{cr}}{k_{c,T_{cr}}})\end{cases} \tag{12}$$

On the basis of the average historical-max temperature of core UHPC ($\bar{T}_{c,max}$) obtained by Eq. (9) and the equivalent high temperature reduction factor ($\bar{k}_{c,T_{max}}$) of core UHPC with 0% and 2% volume of steel fibre calculated by Eq.(12), the strength of core UHPC with 0% and 2% volume of steel fibre after elevated temperature ($\bar{f}_{ck,T_{max}}$) were obtained using Eq.(5).

4.3 The residual strength of the UHPCFST stub columns

A): At room temperature

Based on the uniform theory and extensive parametric studies, Han proposed Eq.(13) to calculate the compressive strength of circular normal CFST columns at room temperature[48]. In the authors' previous work[49], based on the theory of elasticity, a unified formulation was proposed to predict the compressive strength of circular normal CFST columns at room temperature, which is expressed as Eq.(14).

$$N_0=(1.14+1.02\xi)\,f_{ck}A_{sc} \tag{13}$$

$$N_0=\left(1+0.5\frac{\xi}{1+\xi}\right)\left(f_sA_s+f_{ck}A_c\right)=(1+1.5\xi)\,f_{ck}A_c \tag{14}$$

where $A_{sc} = A_s + A_c$; $\xi = (f_s \cdot A_s)/(f_{ck} \cdot A_c)$ is the confinement coefficient; f_s and f_{ck} are the yield strength of steel tube and the prism compressive strength of concrete, respectively;

The restraining action of the steel tube is smaller to the core UHPC due to the lower expansion of UHPC compared with normal concrete[50], therefore the formula for predicting the compressive strength of steel tube filled with normal concrete can not be applied to the UHPCFST directly. The test results of the UHPCFST stub column from Zhu [51], Xiong [52] , Wu [50] and this paper were used to obtain the design formula, as expressed in Eq.(15) and Eq.(16). As shown in Fig. 19, the predicted results agree well with the test results.

$$N_0 = (0.98 + 0.85\xi) f_{ck} A_{sc} \tag{15}$$

$$N_0 = \left(1 + 0.24\frac{\xi}{1+\xi}\right)(f_s A_s + f_{ck} A_c) = (1 + 1.24\xi) f_{ck} A_c \tag{16}$$

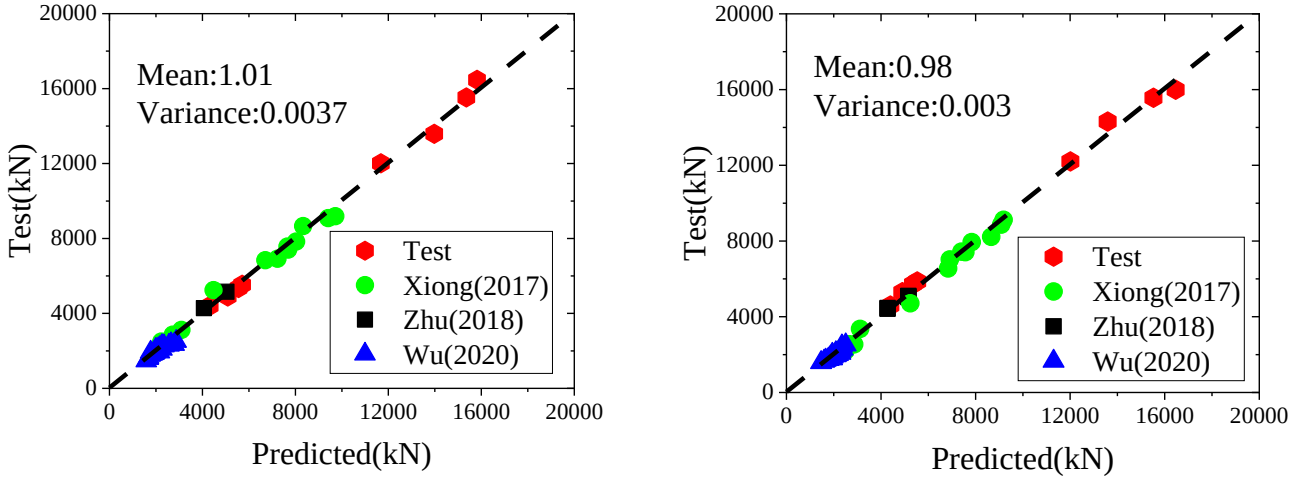

a) Based on Han's formula b) Based on Yu's formula

Fig. 19 The comparison of load bearing capacity of UHPCFST between test and predicted results at room temperature

B): After elevated temperatures

Based on the assumptions in section 4.1, the method proposed by Han [48] and Yu[49] for predicting the compressive strength of UHPCFST stub columns at room temperature can be extended to post fire conditions, as expressed in Eq.(17) and Eq.(18), respectively.

$$N_{T_{max}} = (0.98 + 0.85\xi_{T_{max}}) \cdot \bar{f}_{ck,T_{max}} A_{sc} \tag{17}$$

$$N_{T_{max}} = \left(1 + 0.24\frac{\xi_{T_{max}}}{1+\xi_{T_{max}}}\right)\left(f_{s,T_{max}} A_s + \bar{f}_{ck,T_{max}} A_c\right) \tag{18}$$

where $\xi_{T_{max}} = (f_{s,T_{max}} \cdot A_s)/(\bar{f}_{ck,T_{max}} \cdot A_c)$ is the confinement coefficient after being exposed to elevated temperatures.

Fig. 20 shows the comparison of the residual capacity of UHPCFST stub columns between tested and predicted results. It can be seen that most test results are slightly higher than the predicted results, and the average ratios of the analytical predictions to the experimental results are 1.07 for Eq. (15) and 1.08 for Eq. (16) respectively, with their respective variances of 0.004, 0.006. It is because that the simplified equivalent high temperature reduction factor is quite conservative for achieving a safer design. In general, the predicted results match the test data well, indicating that the proposed method is adequate for predicting the post-fire residual bearing capacity of UHPCFST stub columns after elevated temperatures.

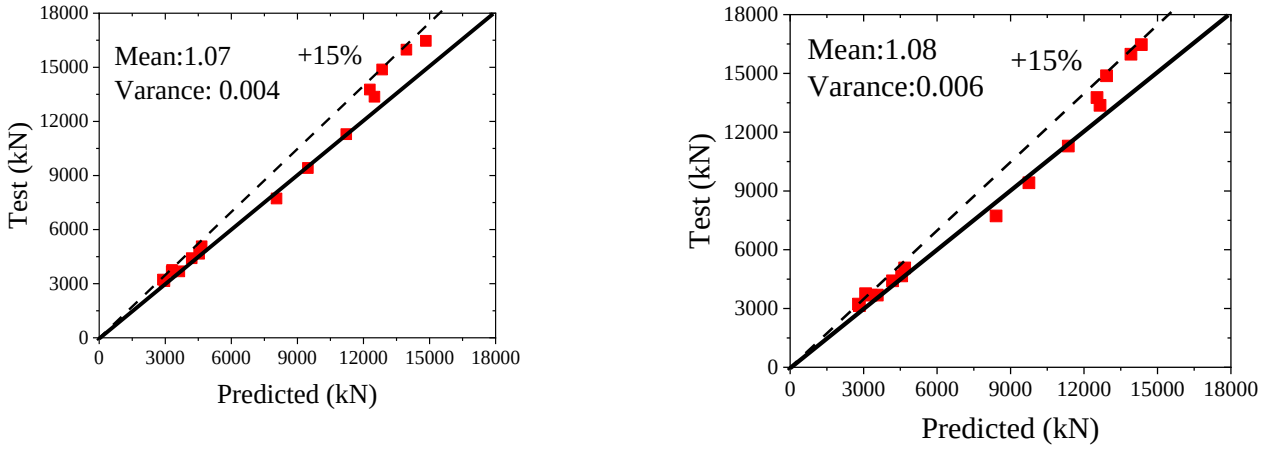

a) Based on Han's formula b) Based on Yu's formula

Fig. 20 The comparison of residual capacity of UHPCFST stub columns between test and predicted results

4.4 Calculation procedure and validation

Six post-fire stub columns from reference [49] were selected to validate the proposed method for predicting the post-fire residual load capacity of UHPCFST specimens. To facilitate design, a step-by-step procedure is summarized as below:

Step1: Calculate average historical-max temperature of steel tube ($\bar{T}_{s,max}$) and core UHPC ($\bar{T}_{c,max}$) using Eq. (8) and Eq. (9), respectively.

Step2: Calculate equivalent strength of the steel ($f_{s,T_{max}}$) tube and the concrete core ($\bar{f}_{ck,T_{max}}$) at the average temperatures from step 1 by using the Eq. (10) and Eq. (12) combing with Eq. (5), respectively.

Step3: Calculate post-fire residual strength of the UHPCFST column under fire using Eq. (15) or Eq. (16).

To better understand the calculation procedure of the proposed method, a worked example for column LC-2-3X from reference [49] is given below as an example. The dimensions and test results are summarised in Table 3.

Step1: For column LC-2-3X in table 3, both m and n are taken as 1 as the raw material does not contain steel fibre or coarse aggregate. The heating-up time is 71 minutes. Substituting those parameters to the Eq. (8) and Eq. (9), eventually the average historical maximum temperature of steel tube $\bar{T}_{s,max}$ and core UHPC $\bar{T}_{c,max}$ were obtained as following:

$$\bar{T}_{s,\max}=\frac{(1\times 71)^{1.22}}{(1\times 71)^{1.22}+18}345\times\log_{10}(8\times 71+1)+20=845\ (℃)$$

$$\bar{T}_{c,\max}=\frac{\left((1\times 71)/(219-2\times 16)^{5}\right)^{0.3}}{\left((1\times 71)/(219-2\times 16)^{5}\right)^{0.3}+0.00035}\times 845+20=696\ (℃)$$

Step2: The equivalent strength of steel tube $f_{s,T_{max}}$ and core UHPC $\bar{f}_{ck,T_{max}}$ after elevated temperatures are calculated using the Eq. (10) and Eq. (12) combing with Eq. (5) based on the average historical-max temperature obtained from Step1.

$$f_{s,T_{\max}}=f_s\times k_{s,T_{\max}}(845)=432\times 0.778=336\ (Mpa)$$

$$\bar{f}_{ck,T_{\max}}=f_{ck}\times\bar{k}_{ck,T_{\max}}(696)=168\times 1.139\frac{1100-696}{1100-500}=129\ (Mpa)$$

Step3: The residual strength of the UHPCFST stub column is obtained based on Eq. (18).

$$N_{T_{\max}} = \left(1+0.24\frac{0.97}{1+0.97}\right)\left(336\times10204+129\times2765\right)=7792\,(kN)$$

Table 3 summarises both the experimental and calculated theoretical residual load capacities of all six UHPCFST stub columns from reference [53]. It is shown that the average ratio of the analytical predictions to the experimental results is 0.94, with a variance of 0.018, which verifies the accuracy of the proposed method once again.

Table 3 Comparison of residual load capacity of UHPCFST between the proposed calculated results and test results in reference[53]

Specimen ID	D	ds	Time	f_s (Mpa)	f_{ck} (Mpa)	Tested capacity（kN）	$\bar{T}_{s,max}$ (^{0}C)	$\bar{T}_{c,max}$ (^{0}C)	$f_{s,T_{max}}$ (Mpa)	$\bar{f}_{ck,T_{max}}$ (Mpa)	$\xi_{T_{max}}$	Predicted capacity（kN）	Ratio
LC-2-3X	219	16	71	432	168	8920	845	697	336	129	0.97	7792	0.87
LC-2-5X	219	16	175	432	168	7080	1029	885	286	69	1.55	5535	0.78
LC-2-6X	219	16	26	432	165	10590	586	458	401	201	0.74	10648	1.01
LC-3-1X	273	16	191	432	164	10271	1045	842	282	80	0.99	8212	0.80
LC-3-2S	273	16	18	418	170	13958	479	329	408	185	0.62	15046	1.08
LC-3-2X	273	16	18	418	170	13969	479	329	408	185	0.62	15046	1.08
Mean													0.94
Variance													0.018
CC-1	133	4.8	90	340	37.92	585	945	802	243	3.8	10	616	0.95
CC-2	133	4.8	90	340	37.92	605	945	802	243	3.8	10	616	0.98

Table 4 Comparison of residual load capacity of normal concrete-filled steel tube columns between the proposed calculated results and test results in reference

Specimen ID	D	ds	Time	f_s (Mpa)	f_{ck} (Mpa)	Tested capacity（kN）	$\bar{T}_{s,max}$ (℃)	$\bar{T}_{c,max}$ (℃)	$f_{s,T_{max}}$ (Mpa)	$\bar{f}_{ck,T_{max}}$ (Mpa)	$\xi_{T_{max}}$	Predicted capacity（kN）	Ratio
CC-1	133	4.8	90	340	37.92	585	945	802	243	3.8	10	616	0.95
CC-2	133	4.8	90	340	37.92	605	945	802	243	3.8	10	616	0.98

Meanwhile, the proposed model has good compatibility and can be extended to predict the post-fire residual strength of normal CFST stub columns by adjusting the corresponding parameters in Eq. (9) based on the thermal parameter of normal concrete and replace the reduce factor Eq. (12) by the reduction factor of normal concrete. Based on the thermal parameter and reduce factor of normal concrete from Eurocode[54] and T/CECS 252-2019[55], n in E(9) is taken as 0.1 and equivalent reduction factor is taken as Eq.(19).

$$\bar{k}_{ck,T_{\max}} = -0.36\left(\frac{\bar{T}_{c,\max}}{1000}\right)-0.95\left(\frac{\bar{T}_{c,\max}}{1000}\right)+1.06 \tag{19}$$

To verify the compatibility of the proposed model, experimental results of post-fire normal concrete-filled steel tube stub columns from Han[12] were selected, and the comparison of residual load capacity of normal concrete-filled steel tube columns between the proposed calculated results and test results were presented in Table 4. It can be found that the proposed calculated results match with test results well, indicating the proposed model have good compatibility.

5 Conclusion and ongoing work

The paper presents the experimental investigation on Twenty-four full-scale UHPCFST stub columns under axial compression after being exposed to elevated temperatures. The failure modes, cross-sectional historical-max

temperatures, axial load-deformation curves, and residual compression of the specimens are analysed. Meanwhile, a hand calculation method for predicting post-fire load capacity of CFST columns based on average historical-max temperatures was proposed with an explicit physical meaning and simple expression. Based on the present study, the following conclusions are drawn:

1） The historical-max temperature of core UHPC shows non-uniform and nonlinear distribution along the concrete depth, and the temperature is higher for the specimens with smaller cross-sectional size and higher content of steel fibre and coarse aggregate;

2） A UHPCFST column has relatively high residual capacity compared with normal CFST, and the influence of historical temperature on the residual capacity of a UHPCFST column is more obvious with the increase of the heating rate and decrease of cross-sectional size;

3） The non-uniform deterioration of concrete can be described as a uniform deterioration by using an equivalent strength of concrete. By doing so, the formula of the compressive strength of the CFST columns after elevated temperatures is unified with the formula at room temperature by replacing the equivalent strength with that after the elevated temperatures;

4） There is still a reserved safety margin of the proposed design method for calculating the residual capacity of UHPCFST using the two-piecewise linear function for the equivalent high temperature reduction factor of concrete strength.

Acknowledge

This study was supported financially by the National Natural Science Foundation of China (Grant NO. 51878518, NO. 52178157).

Reference

[1] Shi CJ, Wu ZM, Xiao JF, Wang DH, Huang ZY, Fang Z. A review on ultra high performance concrete: Part I. Raw materials and mixture design. Constr Build Mater. 2015;101741-51.

[2] Wang C, Yang CH, Liu F, Wan CJ, Pu XC. Preparation of Ultra-High Performance Concrete with common technology and materials. Cem Concr Compos. 2012;34538-44.

[3] Lee NK, Koh KT, Park SH, Ryu GS. Microstructural investigation of calcium aluminate cement-based ultra-high performance concrete (UHPC) exposed to high temperatures. Cement Concrete Res. 2017;102109-18.

[4] Zhu YP, Hussein H, Kumar A, Chen G. A review: Material and structural properties of UHPC at elevated temperatures or fire conditions. Cem Concr Compos. 2021;123104212.

[5] Li Y, Pimienta P, Pinoteau N, Tan KH. Effect of aggregate size and inclusion of polypropylene and steel fibers on explosive spalling and pore pressure in ultra-high-performance concrete (UHPC) at elevated temperature. Cem Concr Compos. 2019;9962-71.

[6] Li Y, Tan KH, Yang EH. Synergistic effects of hybrid polypropylene and steel fibers on explosive spalling prevention of ultra-high performance concrete at elevated temperature. Cem Concr Compos. 2019;96174-81.

[7] Yang J, Peng GF, Zhao J, Shui GS. On the explosive spalling behavior of ultra-high performance concrete with and without coarse aggregate exposed to high temperature. Constr Build Mater. 2019;226932-44.

[8] Zhang D, Liu YC, Tan KH. Spalling resistance and mechanical properties of strain-hardening ultra-high performance concrete at elevated temperature. Constr Build Mater. 2021;266120961.

[9] Tan QH, Gardner L, Han LH, Song TY. Performance of concrete-filled stainless steel tubular (CFSST) columns after exposure to fire. Thin Wall Struct. 2020;149106629.
[10] He A, Liang YT, Zhao O. Behaviour and residual compression resistances of circular high strength concrete-filled stainless steel tube (HCFSST) stub columns after exposure to fire. Eng Struct. 2020;203109897.
[11] Ekmekyapar T, Alhatmey IAH. Post-fire resistance of internally ring stiffened high performance concrete filled steel tube columns. Eng Struct. 2019;183375-88.
[12] Han LH, Huo JS, Wang YC. Compressive and flexural behaviour of concrete filled steel tubes after exposure to standard fire. J Constr Steel Res. 2005;61882-901.
[13] Han L, Yang Y, Yang H, Huo J. Residual strength of concrete-filled RHS columns after exposure to the ISO-834 standard fire. THIN WALL STRUCT. 2002;40991-1012.
[14] Huo JS, Huang GW, Xiao Y. Effects of sustained axial load and cooling phase on post-fire behaviour of concrete-filled steel tubular stub columns. J Constr Steel Res. 2009;651664-76.
[15] Liu FQ, Gardner L, Yang H. Post-fire behaviour of reinforced concrete stub columns confined by circular steel tubes. J Constr Steel Res. 2014;10282-103.
[16] Liu FQ, Yang H, Wang W. Behaviours of concentrically and eccentrically loaded square steel tube confined reinforced concrete slender columns after fire exposure. Thin Wall Struct. 2021;158107155.
[17] Liu FQ, Yang H, Yan R, Wang W. Experimental and numerical study on behaviour of square steel tube confined reinforced concrete stub columns after fire exposure. Thin Wall Struct. 2019;139105-25.
[18] Lyu XT, Zhang T, Liu FQ, Liu YJ. Behaviours of stiffened concrete-filled thin-walled square steel tubular stub columns after non-uniform fire exposure. J Constr Steel Res. 2022;188107031.
[19] Yang H, Han LH, Wang YC. Effects of heating and loading histories on post-fire cooling behaviour of concrete-filled steel tubular columns. J Constr Steel Res. 2008;64556-70.
[20] Yang H, Liu FQ, Gardner L. Post-fire behaviour of slender reinforced concrete columns confined by circular steel tubes. Thin Wall Struct. 2015;8712-29.
[21] Yao Y, Hu XX. Cooling behavior and residual strength of post-fire concrete filled steel tubular columns. J Constr Steel Res. 2015;112282-92.
[22] Abbas H, Al-Salloum Y, Alsayed S, Alhaddad M, Iqbal R. Post-heating response of concrete-filled circular steel columns. KSCE J Civ Eng. 2017;211367-78.
[23] Xue CC, Yu M, Xu H, Xu LH, Saafi M, Ye JQ. Experimental study on thermal performance of ultra-high performance concrete with coarse aggregates at high temperature. Constr Build Mater. 2022;314125585.
[24] Zheng WZ, Wang R, Wang Y. Experimental study on thermal parameter of reactive powder concrete. Journal of Building Structures. 2014;35107-14.
[25] Gong JQ, Deng GQ, Shan B. Performance evaluation of RPC exposed to high temperature combining ultrasonic test: A case study. Constr Build Mater. 2017;157194-202.
[26] Kahanji C, Ali F, Nadjai A, Alam N. Effect of curing temperature on the behaviour of UHPFRC at elevated temperatures. Constr Build Mater. 2018;182670-81.
[27] Zheng WZ, Li HY, Wang Y. Compressive behaviour of hybrid fiber-reinforced reactive powder concrete after high temperature. Mater Design. 2012;41403-9.
[28] Wu F, Xu L, Chi Y, Zeng Y, Deng F, Chen Q. Compressive and flexural properties of ultra-high performance fiber-reinforced cementitious composite: The effect of coarse aggregate. Compos Struct. 2020;236-111810.
[29] Wang T, Yu M, Zhang XP, Ye JQ. Experimental Study on Random Temperature Field of Ultra-High Performance Concrete Filled Steel Tube Columns under Elevated Temperature. Compos Struct. 2022; 289-115445.
[30] Chen S, Zhang R, Jia L, Wang J, Gu P. Structural behavior of UHPC filled steel tube columns under axial loading. Thin Wall Struct. 2018;130550-63.

[31] Zhang R, Chen S, Gu P, Huang Y. Structural behavior of UHPC filled steel tubular columns under eccentric loading. Thin Wall Struct. 2020;1561069-59.
[32] Hoang AL, Fehling E, Lai B, Thai D, Chau NV. Experimental study on structural performance of UHPC and UHPFRC columns confined with steel tube. Eng Struct. 2019;187457-77.
[33] Xu L, Lu Q, Chi Y, Yang Y, Yu M, Yan Y. Axial compressive performance of UHPC filled steel tube stub columns containing steel-polypropylene hybrid fiber. Constr build mater. 2019;204754-67.
[34] GB/T 8162-2018. Seamless steel tubes for structural purposes. Beijing, China, 2018.
[35] Guo Y, Fang C, Zheng Y. Post-fire hysteretic and low-cycle fatigue behaviors of Q345 carbon steel. J Constr Steel Res. 2021;187-106991.
[36] T/CECS 10107-2020. Technical requirements for ultra high performance concrete. Beijing, China: China, Standards Press,2020.
[37] Han LH, Huo JS, Yang YF. Concrete-filled HSS columns after exposure to ISO-834 fire standard. Advances in Steel Structures (ICASS '02). 2002.
[38] Feng P, Cheng S, Bai Y, Ye LP. Mechanical behavior of concrete-filled square steel tube with FRP-confined concrete core subjected to axial compression. Compos Struct. 2015;123312-24.
[39] Peng G, Niu X, Shang Y, Zhang D, Chen X, Ding H. Combined curing as a novel approach to improve resistance of ultra-high performance concrete to explosive spalling under high temperature and its mechanical properties. Cement Concrete Res. 2018;109147-58.
[40] Yu M, Zha XX, Ye JQ, Wang BL. A unified method for calculating fire resistance of solid and hollow concrete-filled steel tube columns based on average temperature. Eng Struct. 2014;7112-22.
[41] Yu M, Hu X, Chi Y, Ye JQ. A unified method for calculating the fire resistance of concrete-filled steel tube with fire protection under combined loading. J Constr Steel Res. 2020;168106003.
[42] Yu M, Pei XY, Xu LH, Ye JQ. A unified formula for calculating bending capacity of solid and hollow concrete-filled steel tubes under normal and elevated temperature. J Constr Steel Res. 2018;141216-25.
[43] Yu M, Xu HM, Ye JQ, Chi Y. A unified interaction equation for strength and global stability of solid and hollow concrete-filled steel tube columns under room and elevated temperatures. J Constr Steel Res. 2018;148304-13.
[44] Lie TT, Irwin RJ. Fire Resistance of Steel Columns Filled with Bar-Reinforced Concrete. J Struct Eng. 1995;121.
[45] Yu M, Zha XX, Ye JQ, Li Y. Fire responses and resistance of concrete-filled steel tubular frame structures. Int J Struct Stab Dy. 2012;10253-71.
[46] Ye QY. Research on fire resistance of ultral-high performance concrete filled circular steel tube column. Wuhan: Wuhan University; 2020.
[47] Wickström U. A very simple method for estimating temperature in fire exposed concrete structures. 1986.
[48] Han LH. Concrete filled steel tubular structure -- Theory and Practice（Third Edition）. Bei Jing: Science Press, 2016.
[49] Yu M, Zha XX, Ye JQ, She CY. A unified formulation for hollow and solid concrete-filled steel tube columns under axial compression. Eng Struct. 2010;321046-53.
[50] Wu FH. Study on mechanical behavior of ultra-high performance concrete with coarse aggregate filled circular steel tube members. Wuhan university; 2020.
[51] Zhu JY, Chan TM. Experimental investigation on octagonal concrete filled steel stub columns under uniaxial compression. J Constr Steel Res. 2018;147457-67.
[52] Xiong MX, Xiong DX, Liew JYR. Axial performance of short concrete filled steel tubes with high- and ultra-high-strength materials. Eng Struct. 2017;136494-510.
[53] Lv XT. Residual Load Capacity and Experimental Research on Short Steel Tube Infilled with High Strength Concrete Column Post-Fire. 2018, Southeast University.

[54] Institution BS. EN 1994-1-2:2005, Design of Composite Steel and Concrete Structures Part 1.2: General Rules, Structural Fire Design. Brussels2005.
[55] T/CECS 252-2019, Standard for appraisal of engineering structures after fire. Beijing, China: China Architecture & Building Press, 2109.